PostPrint. Bingbing Yang et al. Journal of Membrane Science 628 (2021) 119264
https://doi.org/10.1016/j.memsci.2021.119264

Super selective ammonia separation through hybrid membranes with functionalized ionic liquids

Bingbing Yang [a,b], Lu Bai [a], Liyuan Deng [d], Shaojuan Zeng [a], Jiuli Han [a,b], Xiangping Zhang [a,b,c*]

[a] CAS Key Laboratory of Green Process and Engineering, State Key Laboratory of Multiphase Complex Systems, Beijing Key Laboratory of Ionic Liquids Clean Process, Institute of Process Engineering, Chinese Academy of Sciences, Beijing 100190, China.

[b] School of Chemical Engineering, University of Chinese Academy of Sciences, Beijing 100049, China.

[c] Zhengzhou Institute of Emerging Industrial Technology, Zhengzhou 450000, China

[d] Department of Chemical Engineering, Norwegian University of Science and Technology, 7491 Trondheim, Norway

*Correspondence and requests for materials should be addressed to xpzhang@ipe.ac.cn;

PostPrint. Bingbing Yang et al. Journal of Membrane Science 628 (2021) 119264
https://doi.org/10.1016/j.memsci.2021.119264

Abstract

Efficient separation and recovery of ammonia (NH_3) is essential for environmental protection and resource utilization. In this work, hybrid membranes for NH_3 separation were developed by combining the unique features of protic ionic liquids (ILs) and a midblock-sulfonated block copolymer. The functionalized ILs ([2-Mim][NTf_2] and [Im][NTf_2]) with ammonia interaction sites were incorporated into the Nexar^{TM} matrix, which greatly improves the affinity for NH_3 over N_2 and H_2. Benefited from the self-assembly of the block copolymer, the incorporated ILs in the hybrid membranes induce rearrangement of the micro-structure, altering the Nexar morphology primarily consisting of lamellae. More continuous ionic domains with well-distributed ILs were created in the hybrid membranes, contributing to forming interconnected channels for enhanced gas transport. Nexar/[Im][NTf_2]-25 wt% membrane achieves the highest NH_3 permeability of 3565 Barrer and a maximum NH_3/N_2 and NH_3/H_2 ideal selectivity of 1865 and 364, respectively. The significantly enhanced NH_3 permeation compared with the neat Nexar membrane indicates the positive role of IL in the hybrid membrane.

Keywords: Ionic liquids; Hybrid membranes; Ammonia separation; Nexar; Ionic domains

1. Introduction

Ammonia (NH_3) is one of the most widely used chemicals in industries. The primary utilization of NH_3 is the production of nitrogen-containing compounds such as fertilizers, pharmaceuticals, and explosives[1, 2]. In recent decades, in particular, NH_3 has been received increasing interest as an attractive energy carrier to power generation [3-7], which demands carbon-free energy production to relieve the greenhouse effect. However, along with NH_3 production or utilization, global ammonia emissions increase[8]. NH_3-containing gases come from various sources, such as ammonia synthesis, urea production, and metal smelting. The direct emission of NH_3 will cause a severe loss of NH_3 resources. In addition, as an alkaline pollutant with a pungent odor and corrosivity, NH_3 causes the formation of NH_4^+ particulates and aerosols in the atmosphere[9, 10], leading to problems in both air quality and human health. Water scrubbing and acid scrubbing are widely used to deal with exhausted NH_3-containing gases to address the issues mentioned above. However, these technologies are inevitably facing high water consumption, low values of end-products, and sewage pollution[11].

Ionic liquids (ILs), with extremely low vapor pressure, tunable structures and properties, and excellent thermal stability, have been reported to be potential ammonia absorbents for high-efficient ammonia separation [12]. Yokozeki et al. [13, 14] first reported the NH_3 absorption performance of imidazolium-based conventional ILs with variable cations and anions. Shang et al. [15, 16] confirmed the high NH_3 capacity of protic ionic liquids (PILs) through hydrogen-bond interaction between NH_3 and imidazole ring. Zeng et al. [17] further presented a series of metal ionic liquids (MILs) for efficient absorption of NH_3 through Lewis acid-base and synergic hydrogen bond interactions. Although ILs exhibit high NH_3 capacity and good recyclability during the NH_3 absorption process, the utilization of most ILs in NH_3 absorption still suffers from problems caused by the relatively high viscosity during absorption. The high cost of the absorbents in a large amount is also an issue. Incorporating ILs into solid support to make new composites such as IL-based membranes has been proposed as one of effective approaches to take the full advantages of the excellent properties of the new NH_3-seperation ILs while avoiding their problems.

Researches have indicated that incorporating ILs into a polymer matrix to generate IL/polymer hybrid membranes could obtain promising gas separation materials[18]. IL/polymer hybrid membranes have been developed for efficient gas separation, including CO_2 separation[19-22] and O_2/N_2 separation[23]. According to the investigation by Moulin et al. [24], the property of ILs plays a significant role in

determining the gas separation performance of membranes. For example, higher CO_2 solubility in ILs and higher IL content can improve CO_2 transport in the membranes, contributing to better CO_2 separation properties. In this case, it is reasonable to assume that fabricating hybrid membranes by incorporating ILs with NH_3-affinitive moieties is a practical approach to achieve excellent NH_3 separation performance.

According to literature, block copolymers are considered a suitable class of material for NH_3 separation, mainly because of their ability to self-assemble into well-defined nanostructures that benefit gas transport[25-27]. Nexar^{TM}, a commercially available sulfonated pentablock copolymer, has received remarkable attention in membrane separation as a membrane material [28-30]. The polymer maintains good mechanical stability and chain flexibility, benefited by the rigid end blocks (tert-butyl styrene and ethylene-alt-propylene). The middle-sulfonated block generates hydrophilic domains in the polymeric membrane, acting as channels for polar molecules transport[26, 31]. Various studies reveal the transport properties of the membranes largely depend on its morphology, which can be tuned by the solvent-casting process[30, 32].

Moreover, Dai et al. [33] reported the IL-induced nanostructural transformation in Nexar/[Bmim][BF_4] hybrid membranes, which favors CO_2 transport. Thus, to further explore the potential of Nexar/ILs, hybrid membranes for various gas separation applications using different types of ILs with specific features may result in positive outcomes. For instance, it is promising to improve NH_3 permeation through a membrane by applying NH_3-affinitive ILs in a hybrid membrane. Moreover, the effect of ILs on morphology and separation properties of the hybrid membranes is worthy of being investigated.

In this work, Nexar/IL hybrid membranes with optimized nanostructure for enhanced NH_3 separation were fabricated by incorporating functionalized ILs within the midblock-sulfonated block copolymer matrix. 2-methylimidazolium bis (trifluoromethylsulfonyl)imide ([2-Mim][NTf_2]) and imidazolium bis (trifluoromethylsulfonyl)imide ([Im][NTf_2]) were chosen because that they exhibit satisfying NH_3 solubility through hydrogen bonding interaction between the NH_3 and IL molecules. The bulk properties and nanostructures of the hybrid membranes were characterized by Fourier transform infrared spectroscopy (FT-IR), thermogravimetric analysis (TGA), scanning electron microscopy (SEM), transmission electron microscope (TEM), energy dispersive spectrometer (EDS), and small-angle X-ray scattering (SAXS). Single-gas permeabilities of the membranes with different IL structures and various IL content were measured. The influence of ILs incorporation on the morphology and separation performance of the hybrid membranes was investigated.

2. Experimental

2.1. Chemicals and Materials

The analytical grade reagents, including hydrochloric acid (36-38%), ethyl acetate (99.5%), dichloromethane (99.5%), and tetrahydrofuran (THF, 99.9%), were supplied by Beijing Chemical Company (China). Lithium bis (trifluoromethylsulfonyl)imide ($LiNTf_2$), 2-Methylimidazole (98%) and Imidazole (99%) were all purchased from Aladdin Industrial Corporation. All the chemicals above were directly used without further purification. The TEM staining agents were lead citrate solution from Ruixin Company (China). Ultrapure water was obtained from the Milli-Q Direct 8 water purification system. The polymer used in this work is poly[tert-butylstyrene-b-(ethylene-alt-propylene)-b-(styrene-costyrenesulfonate)-b-(ethylene-alt-propylene)-b-tert-butylstyrene] (TS-EP-sS-EP-TS) pentablock ionomer, commercially named Nexar™. The chemical structure of the polymer is shown in Scheme 1. Commercial Nexar™ MD 9200 with an Ion Exchange Capacity (IEC) of 2.0 meq/g were purchased from Kraton Company (USA). NH_3 (99.999%), N_2 (99.999%), and H_2 (99.999%) were supplied by Beijing Beiwen Gas Factory (China).

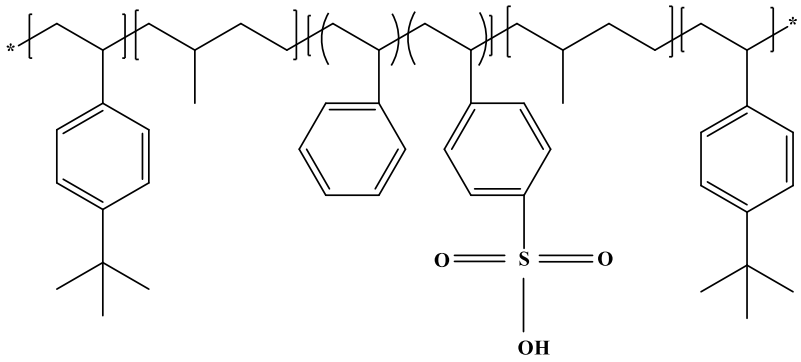

Scheme. 1. Chemical structure of Nexar™

2.2. Ionic liquids synthesis

ILs used in this work were in-house made. [2-Mim][NTf_2] and [Im][NTf_2] were synthesized as reported in our prior work [16]. The structures are shown as Scheme 2. The brief procedure of the synthesis of [2-Mim][NTf_2]) is summarized as follows: Firstly, 2-methylimidazolium chloride ([2-Mim]Cl) was obtained through the reaction between 2-Methylimidazole and HCl, after which the product was washed and dried. Then the anion of [2-Mim]Cl was replaced by $[NTf_2]^-$ offered by $LiNTf_2$. The ultra-pure water was applied to wash impurities in ILs until there was no precipitate when tested with silver nitrate ($AgNO_3$) solution. After a purification process to get rid of residual the most raw materials and water, the target IL was stored in a dry container to be used in membrane preparation.

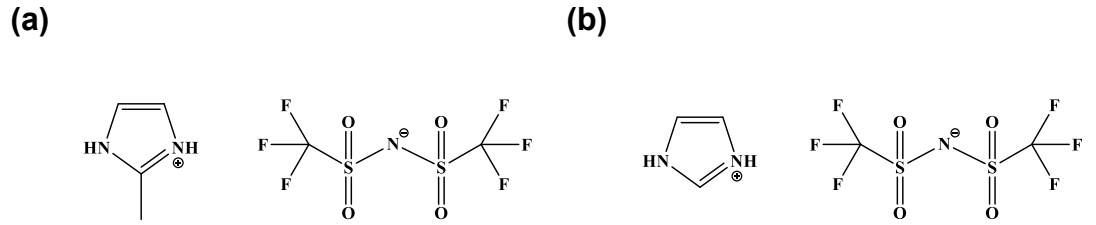

Scheme 2. Structures of (a) [2-Mim][[NTf_2] and (b) [Im][NTf_2]

2.3. Membranes preparation

A calculated amount of IL was first mixed with the desired amount of THF by continuous stirring for at least 2h to promote the dissolution of the IL. Then the polymer was added to the solution, and the mixture was stirred for 4 h again. The obtained mixture was then used for solvent casting in a Teflon module, where a glass petri dish was covered at the top to slow down the rate of evaporation. After at least 2 days, the membrane was dried under vacuum for 12 h. The process was all under ambient temperature.

2.4. Membrane Characterization

Fourier transform infrared spectra (FT-IR, Thermo, Nicolet 380 spectrometer, USA) was used to characterize the chemical spectra of ILs. The FT-IR spectra of the membranes were conducted in attenuated total reflectance (ATR) mode, and the range was from 650 to 4000 cm^{-1}. Thermogravimetric Analysis (TGA, Shimadzu, DTG-60H) was employed under the N_2 atmosphere from ambient temperature to 600 ℃ at the constant heat rate of 10 ℃/min to analyze the thermal stability of membranes and ILs. The membrane morphology was observed by scanning electron microscopy (SEM, HITACHI, SU8020) at 0.9 kV. For cross-sectional observation, the samples were broken in liquid nitrogen. Energy dispersive spectrometer (EDS) was used to detect the distribution of feature elements of ILs in mapping mode, and the membranes were with gold-spraying for no more than 10 s at 5 mA before analysis. The microstructures of membranes were also obtained by transmission electron microscope (TEM, JEOL JEM-2100F) at 200 kV. Films were sliced into ultraslices under liquid nitrogen temperature, after which they were stained by lead citrate and drying. Small-angle X-ray scattering (SAXS, Xenocs, Nano-inXider) was detected by a Dectris Pilatus 3 detector under vacuum and ambient temperature. The wavelength of X-ray (λ) was 0.154 nm, and the scattering sector is shown as $q = (4\pi/\lambda)\sin\theta$, where 2θ represents the scattering angle. The distance (D) was calculated by $D=2\pi/q$.

2.5. Gas permeation measurement

A homemade apparatus was used to measure the gas permeation of the membranes

by a variable pressure, constant volume method, as shown in Fig.c S1. The tests were conducted at room temperature, 1 bar feed pressure. For each test, a membrane was sealed in a membrane module with an effective permeation area of 4.9 cm^2. For each membrane, three samples were tested. The average values from the measurements were used to determine the permeation properties and analyze deviations and error bars.

The permeation coefficient was calculated using the following equation:

$$P = \frac{V_d}{RTA} \times \frac{l}{(p_u - p_d)} \times \left[\left(\frac{dp_d}{dt} \right) - \left(\frac{dp_d}{dt} \right)_{lr} \right] \quad (1)$$

where P is the permeation coefficient in Barrer, V_d represents the downstream volume, R is the universal gas constant, T denotes absolute temperature, A is the effective permeation area, l is the membrane thickness, P_u and P_d are the pressures of upstream and downstream side, and t represents time, respectively. dp_d/dt is the rate of downstream pressure increase at steady state, and $(dp_d/dt)_{lr}$ is the leakage rate.

The ideal selectivity for two gases is determined as:

$$\alpha_{ij} = \frac{P_i}{P_j} \quad (2)$$

where P_i and P_j are the permeation coefficients of pure gas i and j.

The diffusion coefficient (D) was estimated from the time-lag method by using the following equation:

$$D = \frac{l^2}{6\theta} \quad (3)$$

Based on the values of P and D, the solubility coefficient (S) was calculated from

$$S = \frac{P}{D} \quad (4)$$

3. Results and discussion

3.1. Chemical analysis

Fig. 1 (a) and (b) shows the FT-IR spectra of [2-Mim][NTf_2], [Im][NTf_2], the neat Nexar membrane, and the hybrid membranes. The characteristics of hybrid membranes with different ILs and IL contents were both exhibited. After blending the polymer with ILs, the spectra of the hybrid membranes show characteristic peaks of ILs and the polymer, and the intensity of peaks changes with the change of blending composition. For Nexar/[2-Mim][NTf_2]-25 wt% membrane, peaks at 1623 cm^{-1} and 920 cm^{-1} are assigned to N-H deformation vibration and bending vibration out-plane, respectively. Peaks at 1004 cm^{-1}, 1034 cm^{-1}, and 1413 cm^{-1} are the characteristic peaks of -SO_3^- group of the polymer. Peaks at 1126.2 cm^{-1} and 1124.3 cm^{-1} present S=O asymmetric stretchings of the polymer and C-F stretching of the IL, respectively. As for

Nexar/[Im][NTf_2]-25wt% membrane, peaks at 1586 cm^{-1} and 924 cm^{-1} are due to N-H deformation and bending vibration. Peaks at 1005 cm^{-1}, 1035 cm^{-1}, and 1414 cm^{-1} belong to $-SO_3^-$ group. However, only one relatively wide peak around 1130 cm^{-1} appears, which mainly because of the close position of S=O asymmetric stretching and C-F stretching. The wide O-H stretching from the $-SO_3H$ of the polymer, C-H stretching from the polymer and IL, and N-H stretching of IL appear in the range of 2800-3600 cm^{-1}. Additionally, peaks at around 1700 cm^{-1} belong to the C-C stretching of the aromatic ring, which is consistent with the literature[33].

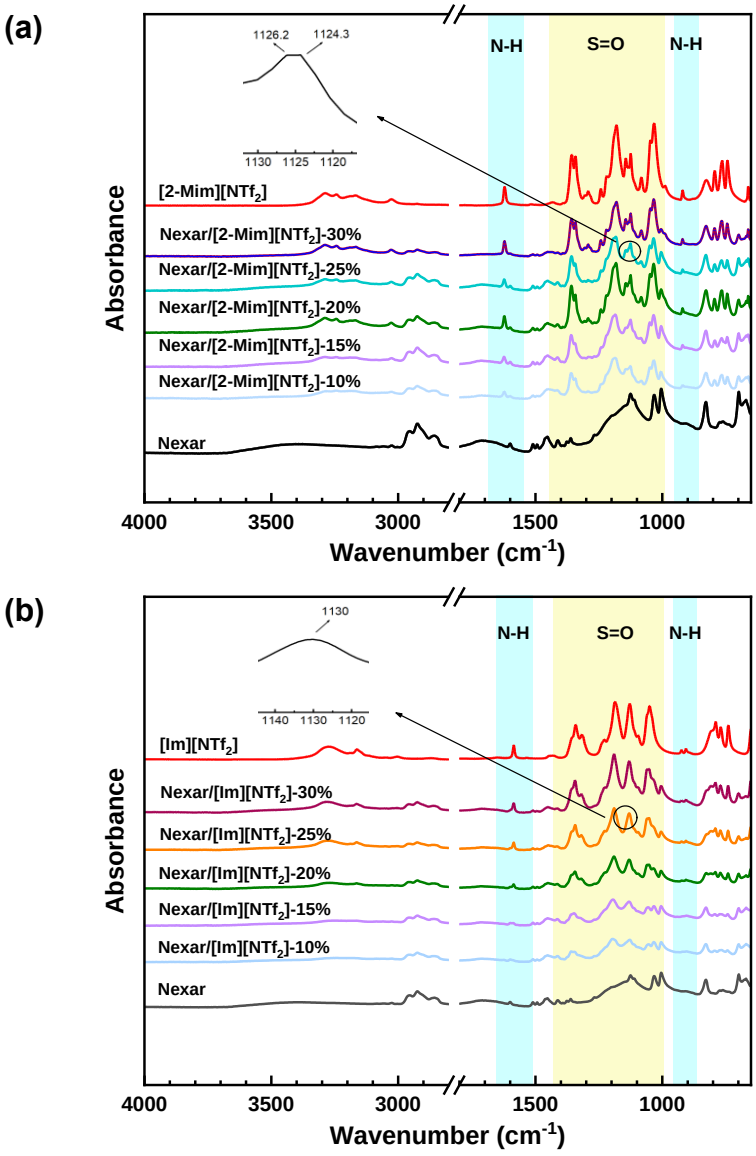

Fig. 1. FT-IR spectra of ILs and the membranes. (a) [2-Mim][NTf_2] and Nexar/[2-Mim][NTf_2] membranes, (b) [Im][NTf_2] and Nexar/[Im][NTf_2] membranes.

3.2. Thermal analysis

The thermal stability of the membranes with different ILs is investigated by TGA, showing the weight loss as a function of temperature (Fig. 2). All hybrid membranes

exhibited a pattern of a four-step decomposition. Thus, as an example, the decomposition of Nexar/[2-Mim][NTf_2] is discussed in detail. The first loss region is between the initial measurement temperature and 150℃, where the atmospheric moisture absorbed by the samples is removed. A similar result is also reported by Scalese et al. [34]. In the second stage, from 150℃ to 350℃, the degradation of the sulfonate groups occurs. The third wight loss between 300℃ to 460℃ is attributed to the decomposition of ILs as well as the Nexar backbone, including *tert*-butylstyrene (TS), ethylene-alt-propylene (EP) and polystyrene (PS) segments. The fourth stage occurs at T>460℃, where the ILs and the membranes gradually decompose. The TGA pattern of the membranes indicates that the incorporation of ILs does not bring about significant changes in the blends.

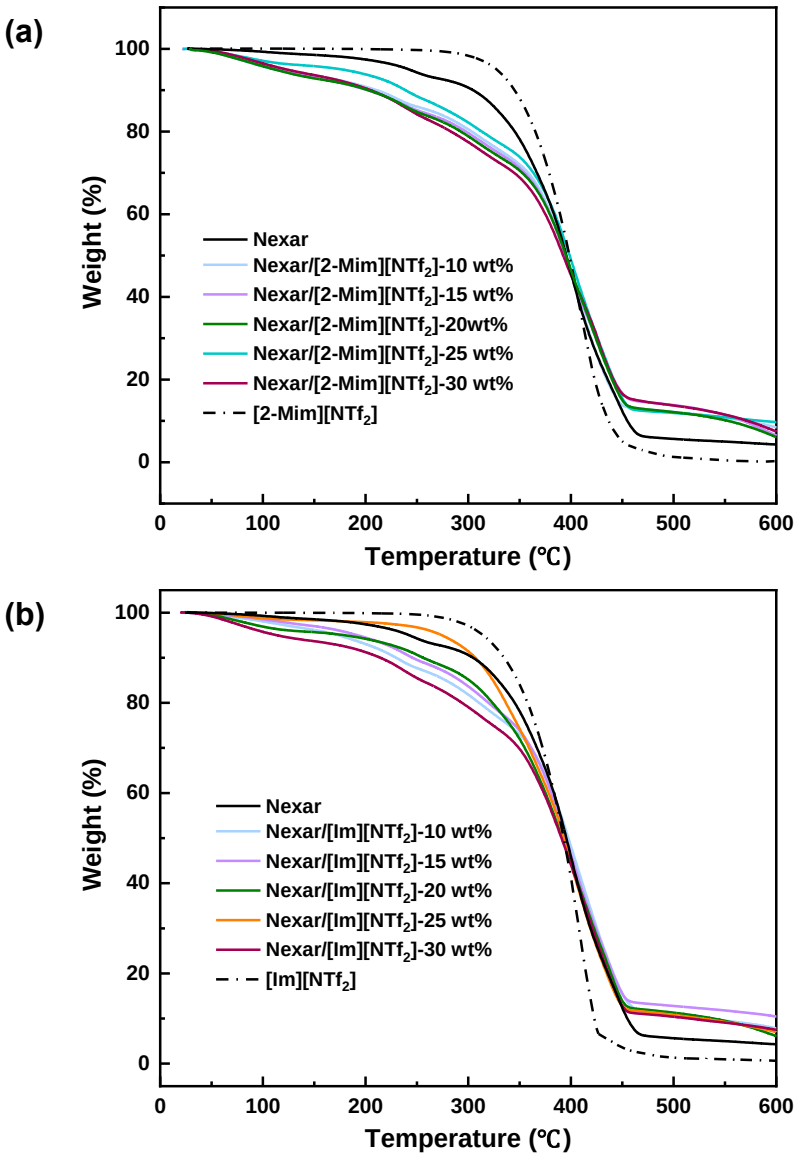

Fig. 2. TGA curves of (a) Nexar/[2-Mim][NTf_2] membranes, the pure Nexar membrane as well as [2-Mim][NTf_2], (b) Nexar/[Im][NTf_2] membranes, the neat Nexar membrane as well as [Im][NTf_2].

3.3. Morphological analysis

Cross-sectional morphologies of the neat Nexar membrane and hybrid membranes with different ILs and different IL content were shown in SEM. The neat Nexar membrane exhibits a lamellar-like morphology, as shown in Fig. S2 (a). With the incorporation of ILs, the hybrid membranes remain similar morphology with the neat Nexar membrane, and the changes in the morphology of hybrid membranes with different IL content are not evident (Fig. 3 (a)-(f) and Fig S2 (b)-(e)). Therefore, elements mapping measurements of fluorine (F) and nitrogen (N) were performed to analyze the dispersion of ILs in the membranes, as shown in Fig. 4 and Fig. S3. ILs are homogeneously dispersed in the matrix, which indicates the good miscibility between ILs and the polymer. Besides, the results may infer that the ILs are not selectively confined in the specific block of the polymer. This observation is further verified in TEM and the corresponding element distribution mappings.

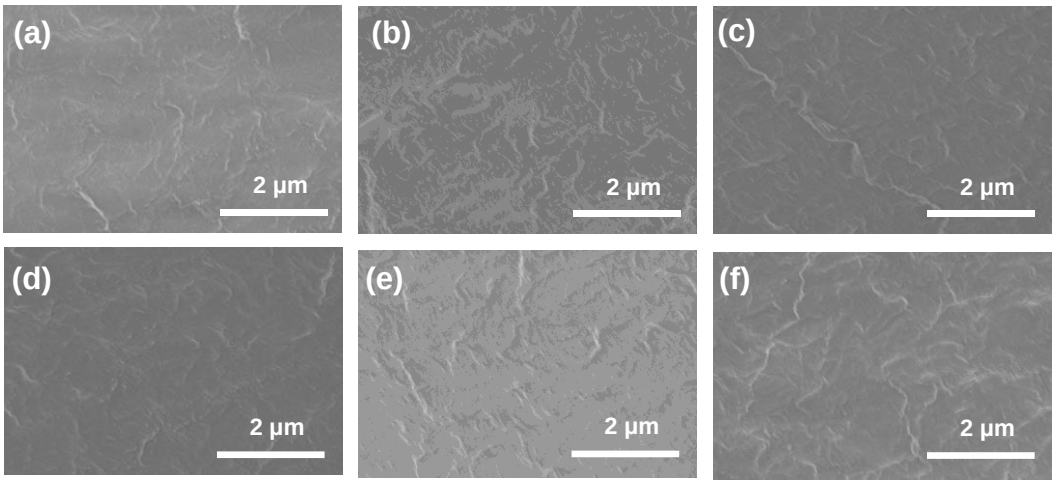

Fig. 4. Cross-sectional SEM images of (a) Nexar/[2-Mim][NTf_2]-10 wt%, (b) Nexar/[2-Mim][NTf_2]-25 wt%, (c) Nexar/[2-Mim][NTf_2]-30 wt%, (d) Nexar/[Im][NTf_2]-10 wt%, (e) Nexar/[Im][NTf_2]-25 wt%, and (f) Nexar/[Im][NTf_2]-30 wt%.

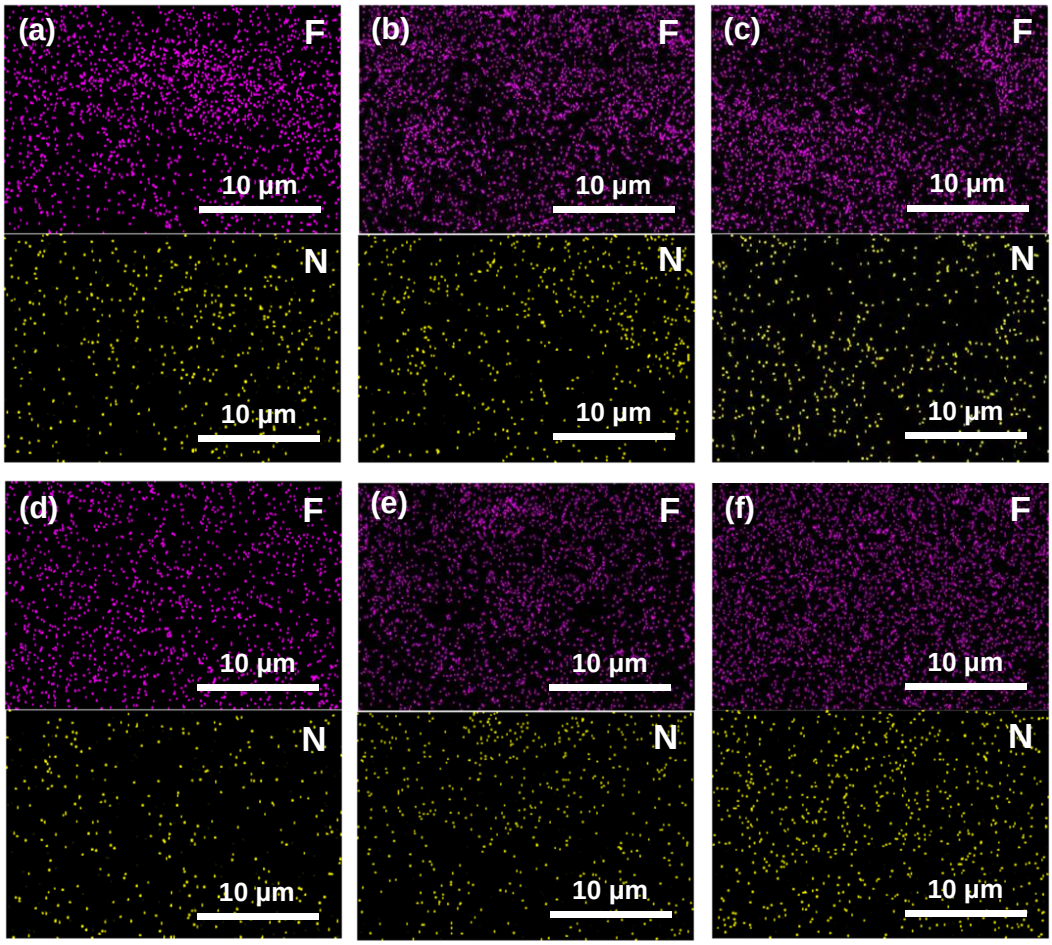

Fig. 4. Element distribution mappings of (a) Nexar/[2-Mim][NTf_2]-10 wt%, (b) Nexar/[2-Mim][NTf_2]-25 wt%, (c) Nexar/[2-Mim][NTf_2]-30 wt%, (d) Nexar/[Im][NTf_2]-10 wt%, (e) Nexar/[Im][NTf_2]-25 wt%, and (f) Nexar/[Im][NTf_2]-30 wt% in SEM.

TEM images of the nanoscale morphologies of the hybrid membranes are presented in Fig. 5. In Fig. 5(a), the Nexar/[2-Mim][NTf_2]-25 wt% membrane exhibits a hybrid nanostructure consisting of lamellae and hexagonally-packed cylinders, of which the lamellar morphology is dominating. The periodicity measured for the lamellae is 35.1 nm, and the ion-rich lamellae of the polymer are thinner than the nonpolar lamellae. Besides, the cylinders are composed of TS and EP blocks with the microdomain periodicity of 36.5 nm. In Fig. 5 (b), the TEM image of Nexar/[Im][NTf_2]-25 wt% membrane also demonstrates a combination of lamellae and cylinders. Microdomain periodicities of lamellae and cylinders are 34.7 nm and 36.0 nm, respectively. According to the results of element distribution mappings of Sulfur (S), F and N (Fig. 6), the ILs are dispersed in both sulfonated and unsulfonated domains of the polymer instead of locating in the specific domain, which is because that the anion of ILs is hydrophobic while the proton on the imidazolium ring increases the polarity. The homogenous dispersion of ILs helps make the ionic microdomains consisting of ILs and the sulfonated domains of the polymer more continuous.

Therefore, the more interconnected channels will favor gas transport in the hybrid membranes.

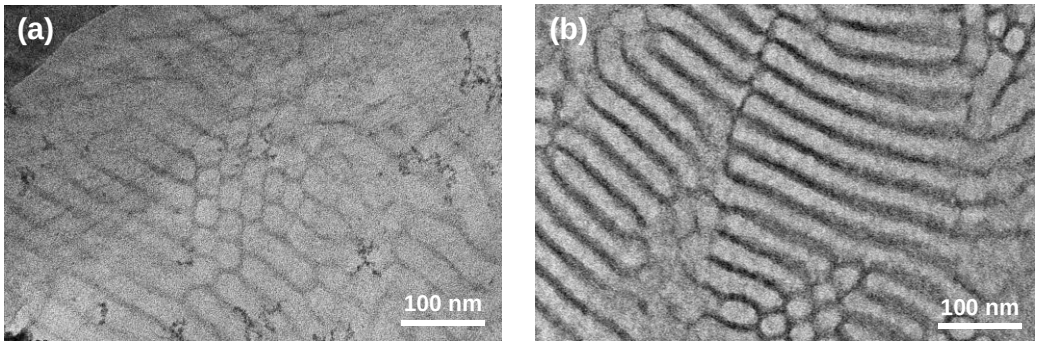

Fig. 5. TEM images of (a) Nexar/[2-Mim][NTf_2]-25 wt%, (b) Nexar/[Im][NTf_2]-25 wt%.

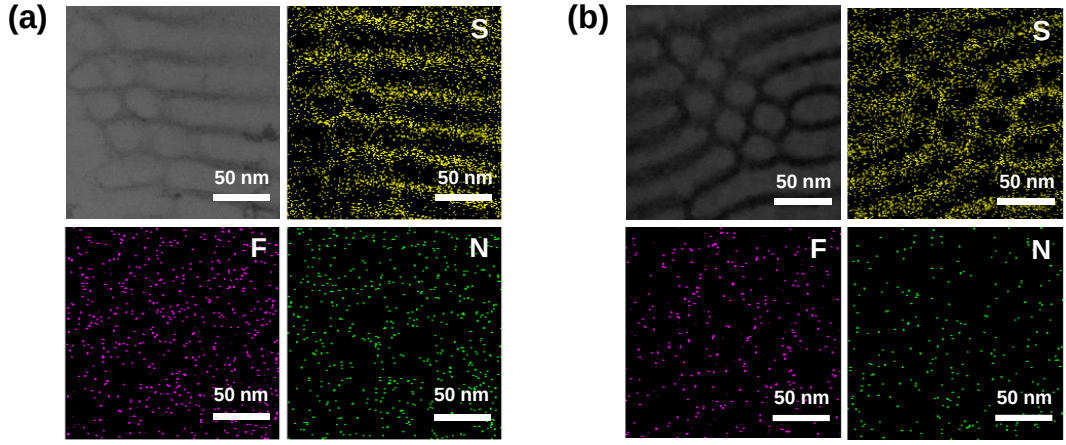

Fig. 6. Elemental mapping images of (a) Nexar/[2-Mim][NTf_2]-25 wt% and (b) Nexar/[Im][NTf_2]-25 wt% in TEM.

The corresponding SAXS profiles provide the microdomain arrangements of hybrid membranes and the neat Nexar membrane (Fig. 7 and Table S1). All membranes exhibit peaks at q*(the primary scattering peak) and 2q*, indicating the existence of lamellae and cylinder [35]. The results confirm the coexisting micro structures in the morphologies observed in TEM images. Nexar/[2-Mim][NTf_2]-10 wt% and Nexar/[Im][NTf_2]-10 wt% possess peaks at around q*, 2q*, 3q*, and 4q*, which implies more ordered nanostructures in the membranes compared with that of the membranes with higher IL contents. The miscrostructure of hybrid membranes with IL content from 15 wt% to 30 wt% change slightly. On the other hand, the location of q* can be used to reveal the microdomain spacing (D) of the membranes. The primary peaks of Nexar/[2-Mim][NTf_2]-10 wt% and Nexar/[Im][NTf_2]-10 wt% shift to a lower q compared with the value of the neat Nexar membrane, and the spacing increase from 41.86 nm to 44.07 nm, implying that the incorporation of ILs into the polymeric matrix promotes nanostructural swelling. A similar phenomenon has been reported in the literature [36]. However, the membranes with higher IL content do not exhibit a

significant change in spacing in comparison with the neat Nexar membrane. Two possible reasons are provided to explain the results: *(i)* ILs are less miscible with the polymeric matrix at high IL content, and *(ii)* the addition of IL affect the intermolecular interaction of polymer chains.

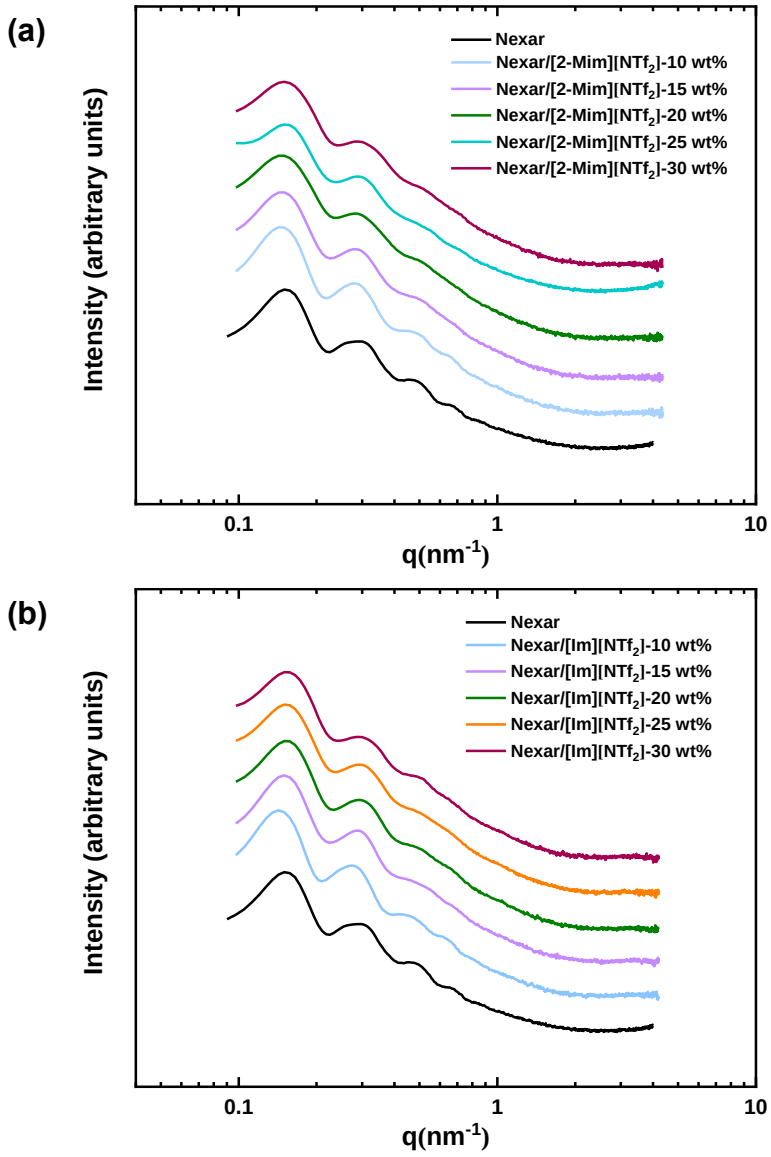

Fig. 7. SAXS profiles collected from (a) Nexar/[2-Mim][NTf_2] membranes and (b) Nexar/[Im][NTf_2] membranes with the neat Nexar membrane.

3.4. Gas permeation properties

NH_3 separation performance of the hybrid membranes was evaluated by single-gas permeation under dry conditions. The NH_3 separation performances of hybrid membranes made of two ILs with different IL contents are displayed in Fig. 8. As expected, by adding ILs of high NH_3 affinity, the hybrid membranes show simultaneous improvement in both NH_3 permeability and selectivity compare with the neat Nexar membrane. Fig. 8 (a) presents the NH_3 permeability of hybrid membranes. With the IL

content increase to xx%, the NH3 permeability increases up to xxx%, demonstrating the positive effect of IL incorporation on NH_3 permeation. As it can be seen, the NH_3 permeability of Nexar/[2-Mim][NTf_2] hybrid membranes increases as IL content increases from 0 to 25 wt%, reaching a maximum of 3248 Barrer. Such a high NH_3 permeability is believed mainly resulted from two improvements: the increased NH3 afifinity by the addition of the specially functionalized ILs, and the optimized microstructure induced by IL that favors the gas transport. Peinemann et al. [31] found that the sulfonated domain of the copolymer would promote polar gas transport through membranes. The incorporation of the IL would form more continuous ionic domains as interconnected channels for NH_3 transport and improve affinity for NH_3 in the hybrid membranes, leading to a significant increment in NH_3 permeability. Nexar/[2-Mim][NTf_2]-30wt% presents lower NH_3 permeability, maybe because that ILs at higher content tend to agglomerate, making the channels less interconnected and then negatively affecting NH_3 transport. Nexar/[Im][NTf_2] membranes perform better in NH_3 permeability than Nexar/[2-Mim][NTf_2] membranes, and the highest NH_3 permeability reaches 3565 Barrer at IL content of 25 wt%, which is an increase of 619% relative to the permeability of the neat Nexar membrane. The better NH_3 permeability of Nexar/[Im][NTf_2] membranes is mainly because that [Im][NTf_2] can provide more effective ammonia interaction sites, forming more interconnected channels for NH_3 transport when compared with [2-Mim][NTf_2].

It is also evident that N_2 permeability and H_2 permeability increase with the increasing IL content, but the increment for these gases is much less than that of NH_3, suggesting that the interconnected channels benefits the transport of all gases, but ILs' much higher affinity for NH_3 compared with N_2 and H_2 favors the NH_3 sorption and results in a much higher increment in NH_3 permeability. As shown in Fig. 8 (b) and (c), ideal NH_3/N_2 selectivities and NH_3/H_2 selectivities of the hybrid membranes are much higher than that of the neat Nexar membrane. NH_3/N_2 selectivities of Nexar/[2-Mim][NTf_2]-25 wt% and Nexar/[Im][NTf_2]-25 wt% are 1662 and 1865, which are 194% and 230% higher than the selectivity of the Nexar membrane. Nexar/[Im][NTf_2]-25 wt% membrane achieves the highest NH_3/H_2 selectivity of 364, reaching an increase of 309% relative to that of the neat Nexar membrane.

(a)

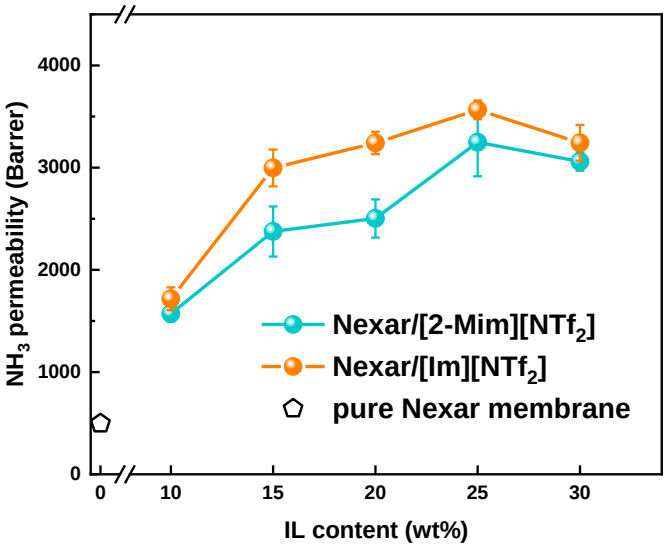
4000
3000
2000
1000
0
NH_3 permeability (Barrer)
0
10
15
20
25
30
IL content (wt%)
Nexar/[2-Mim][NTf_2]
Nexar/[Im][NTf_2]
pure Nexar membrane

(b)

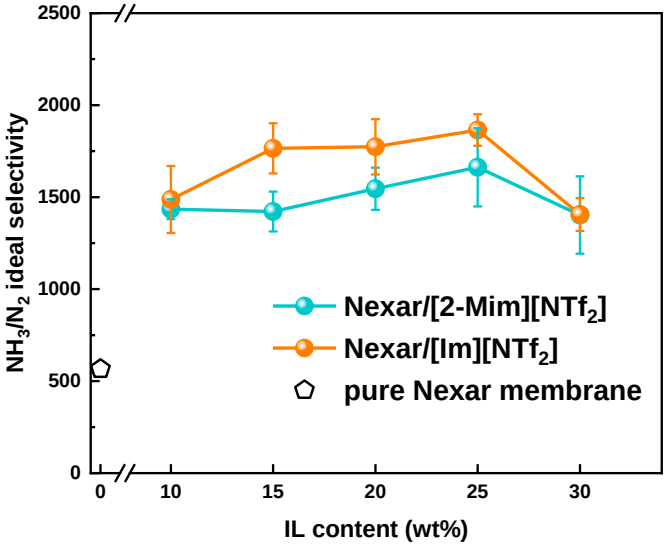
2500
2000
1500
1000
500
0
NH_3/N_2 ideal selectivity
0
10
15
20
25
30
IL content (wt%)
Nexar/[2-Mim][NTf_2]
Nexar/[Im][NTf_2]
pure Nexar membrane

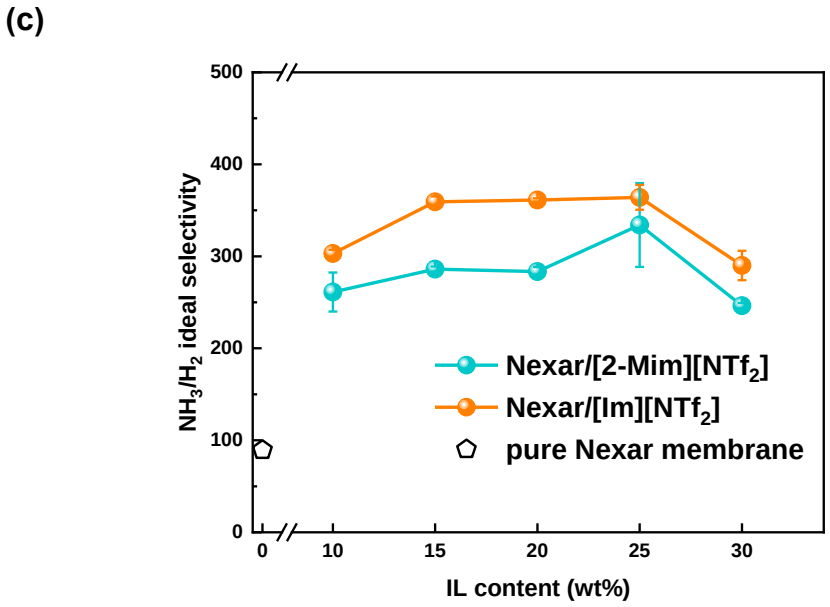

Fig. 8. (a) NH_3 permeability, (b) ideal NH_3/N_2 selectivity, and (c) ideal NH_3/H_2 selectivity of membranes with different IL content.

The diffusion coefficient and solubility coefficient of gases were calculated from the permeation data based on xxxx and analyzed, as shown in Table 1. For hybrid membranes incorporated with ILs, the diffusion coefficients of all gases are significantly enhanced, demonstrating that ILs are favorable for forming channels for transport of all gas. In addition, the diffusion coefficient of NH_3 increases more than that of N_2 and H_2. Diffusion coefficients of hybrid membranes reach the maxima at IL content of 25wt%, after which the value decreases. As the results of the EDS show, the ILs disperse homogenously in the amphiphilic block copolymer matrix. When the IL content increase from 0 to 25 wt%, the more interconnected pathway that boosts gas transport forms. However, when there are up to 30 wt% IL in the matrix, the ILs become less evenly dispersed because of the tendency of the ILs to agglomerate, which affects the connection of the channels for efficient gas transport. The solubility coefficient of NH_3 increases with IL incorporation, and is much higher than that of N_2 and H_2 because ILs are functionalized with sites for efficient absorption of NH_3. Therefore, it is concluded that the increase of NH_3 permeability comes from the enhancement of both diffusion and solubility coefficients, of which NH_3 diffusivity offers more contribution. Meanwhile, the improvement of NH_3 selectivity is mainly attributed to the more favorable NH_3 affinity of the hybrid membranes. Furthermore, diffusion coefficients and solubility coefficients of NH_3 for Nexar/[Im][NTf_2] membranes with IL content of 25 wt% and 30 wt% are higher than those for Nexar/[2-Mim][NTf_2] membranes, most likely because that [Im][NTf_2] has smaller molecular weight so that the IL would provide more sites to locate in the channels at the same IL content.

Table 1
Diffusion coefficients and solution coefficients of N_2, H_2, and NH_3 for the membranes.

Membrane	D_{NH3}	D_{N2}	D_{H2}	S_{NH3}	S_{N2}	S_{H2}	D_{NH3}/D_{N2}	S_{NH3}/S_{N2}	D_{NH3}/D_{H2}	S_{NH3}/S_{H2}
the pure Nexar membrane	2.28	1.55	12.56	2175.00	5.68	4.42	1.48	383.26	0.18	492.08
Nexar/[2-Mim][NTf_2]-10 wt%	5.01	2.45	20.65	3137.18	4.49	2.94	2.05	698.84	0.24	1067.07
Nexar/[2-Mim][NTf_2]-25 wt%	9.86	4.17	29.60	3329.00	4.97	3.37	2.37	670.17	0.33	987.83
Nexar/[2-Mim][NTf_2]-30 wt%	8.09	3.85	27.04	3804.80	5.78	4.65	2.10	658.68	0.30	818.24
Nexar/[Im][NTf_2]-10 wt%	6.21	2.52	22.95	2844.00	4.48	2.44	2.46	634.40	0.27	1165.57
Nexar/[Im][NTf_2]-25 wt%	10.75	4.10	30.92	3368.41	4.55	3.17	2.62	740.64	0.35	1062.59
Nexar/[Im][NTf_2]-30 wt%	8.26	3.92	27.60	3935.00	5.97	4.06	2.11	659.46	0.30	969.21

Diffusion coefficient / 10^{-8} [cm^2/s].
Solubility coefficient / 10^{-3}[cm^3 (STP)/cm^3cmHg].

Compared with various membranes reported in the literature, hybrid membranes in this work exhibit superior NH_3/N_2 separation performance, as shown in Fig. 9 [25-27, 37, 38]. The excellent NH_3 separation performance of the hybrid membrane with both high NH3 permeability and selectivity demonstrates the great potential of the IL-based hybrid membranes in NH_3 separation and purification.

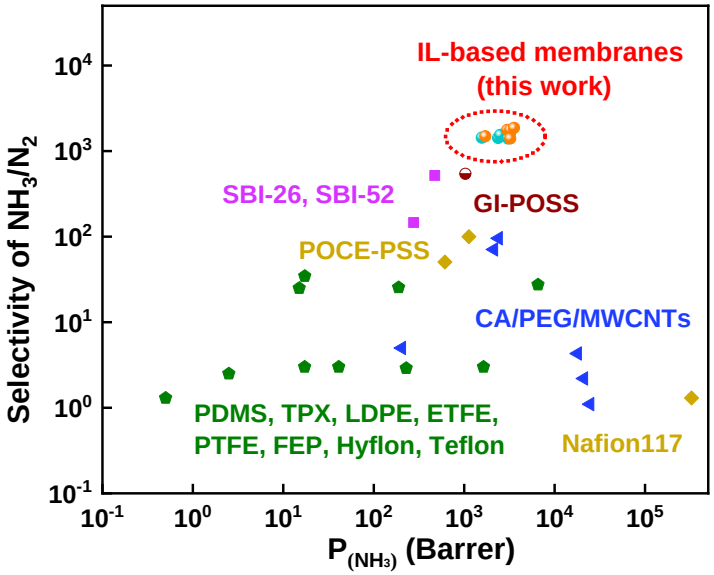

Fig. 9. NH_3/N_2 separation performance of the hybrid membranes compared with the performance of current membranes under dry conditions.

4. Conclusions

Hybrid membranes consisting of functionalized ILs and midblock-sulfonated block copolymer were fabricated for efficient NH_3 separation. The incorpartion of

functionalized ILs with ammonia interaction sites significantly improve the NH_3 affintiy in the hybrid membranes. Morphology analysis reveals that the membranes mainly consist of lamellae coexisting with cylinders, where the ionic microdomains are highly interconnected so that enhanced transport channels are formed for gas transport. Owing to the simultaneous improvement in NH_3 solubility and diffusivity, Nexar/[Im][NTf_2]-25 wt% membrane exhibits the highest NH_3 permeability of 3565 Barrer with NH_3/N_2 and NH_3/H_2 ideal selectivity of up to 1865 and 364, which is superior to the separation performance of all the membranes according to the literature. Meanwhile, applying ILs with more ammonia interaction sites and increasing IL content in the membranes are favorable for improving NH_3 separation performance.

In summary, this work provides an efficient approach to fabricate hybrid membranes incorporated with ILs for NH_3 separation. The outstanding NH_3 performance of the hybrid membranes may bring in the industrial potential for membrane technology in NH_3 separation applications.

Acknowledgments

This work was financially supported by the National Natural Science Foundation of China (21978306), the Science Fund for Creative Research Groups of the National Natural Science Foundation of China (21921005), and the International Partnership Program of the Chinese Academy of Sciences (122111KYSB20190029).

References

[1] R.F. Service, LIQUID SUNSHINE, Science, 361 (2018) 120-123.
[2] K. Kugler, B. Ohs, M. Scholz, M. Wessling, Towards a carbon independent and CO_2-free electrochemical membrane process for NH_3 synthesis, Phys. Chem. Chem. Phys., 16 (2014) 6129-6138.
[3] A. Valera-Medina, H. Xiao, M. Owen-Jones, W.I.F. David, P.J. Bowen, Ammonia for power, Prog. Energy Combust. Sci., 69 (2018) 63-102.
[4] D.W. Kang, J.H. Holbrook, Use of NH_3 fuel to achieve deep greenhouse gas reductions from US transportation, Energy Reports, 1 (2015) 164-168.
[5] P. Xie, Y. Yao, Z. Huang, Z. Liu, J. Zhang, T. Li, G. Wang, R. Shahbazian-Yassar, L. Hu, C. Wang, Highly efficient decomposition of ammonia using high-entropy alloy catalysts, Nat. Commun., 10 (2019).
[6] H.A. Lara-Garcia, J. Arturo Mendoza-Nieto, H. Pfeiffer, L. Torrente-Murciano, COx-free hydrogen production from ammonia on novel cobalt catalysts supported on 1D titanate nanotubes, Int. J. Hydrogen Energy, 44 (2019) 30062-30074.
[7] Y. Shen, R. Abedin, F.R. Hung, On the Performance of Confined Deep Eutectic Solvents and Ionic Liquids for Separations of Carbon Dioxide from Methane: Molecular Dynamics Simulations, Langmuir, 35 (2019) 3658-3671.

[8] A.H. Berner, J. David Felix, Investigating ammonia emissions in a coastal urban airshed using stable isotope techniques, Sci. Total Environ., 707 (2020) 134952.
[9] W. Liu, B. Wu, X. Bai, S. Liu, X. Liu, Y. Hao, W. Liang, S. Lin, H. Liu, L. Luo, S. Zhao, C. Zhu, J. Hao, H. Tian, Migration and Emission Characteristics of Ammonia/Ammonium through Flue Gas Cleaning Devices in Coal-Fired Power Plants of China, Environ. Sci. Technol., 54 (2020) 390-399.
[10] Z.Y. Zhang, Y. Zeng, N.J. Zheng, L. Luo, H.W. Xiao, H.Y. Xiao, Fossil fuel-related emissions were the major source of NH_3 pollution in urban cities of northern China in the autumn of 2017, Environ. Pollut., 256 (2020) 8.
[11] C. Zhang, J. Ma, T.D. Waite, The impact of absorbents on ammonia recovery in a capacitive membrane stripping system, Chem. Eng. J., 382 (2020) 122851.
[12] S. Zeng, Y. Cao, P. Li, X. Liu, X. Zhang, Ionic liquid-based green processes for ammonia separation and recovery, Current Opinion in Green and Sustainable Chemistry, (2020) 100354.
[13] A. Yokozeki, M.B. Shiflett, Ammonia Solubilities in Room-Temperature Ionic Liquids, Ind. Eng. Chem. Res., 46 (2007) 1605-1610.
[14] A. Yokozeki, M.B. Shiflett, Vapor–liquid equilibria of ammonia+ionic liquid mixtures, Applied Energy, 84 (2007) 1258-1273.
[15] D. Shang, X. Zhang, S. Zeng, K. Jiang, H. Gao, H. Dong, Q. Yang, S. Zhang, Protic ionic liquid [Bim][NTf_2] with strong hydrogen bond donating ability for highly efficient ammonia absorption, Green Chem., 19 (2017) 937-945.
[16] D. Shang, S. Zeng, X. Zhang, X. Zhang, L. Bai, H. Dong, Highly efficient and reversible absorption of NH3 by dual functionalised ionic liquids with protic and Lewis acidic sites, J. Mol. Liq., (2020) 113411.
[17] S. Zeng, L. Liu, D. Shang, J. Feng, H. Dong, Q. Xu, X. Zhang, S. Zhang, Efficient and reversible absorption of ammonia by cobalt ionic liquids through Lewis acid–base and cooperative hydrogen bond interactions, Green Chem., 20 (2018) 2075-2083.
[18] D.M. Correia, L.C. Fernandes, P.M. Martins, C. García-Astrain, C.M. Costa, J. Reguera, S. Lanceros-Méndez, Ionic Liquid–Polymer Composites: A New Platform for Multifunctional Applications, Adv. Funct. Mater., (2020) 1909736.
[19] J. Deng, L. Bai, S. Zeng, X. Zhang, Y. Nie, L. Deng, S. Zhang, Ether-functionalized ionic liquid based composite membranes for carbon dioxide separation, RSC Adv., 6 (2016) 45184-45192.
[20] M. Li, X. Zhang, S. Zeng, L. Bai, H. Gao, J. Deng, Q. Yang, S. Zhang, Pebax-based composite membranes with high gas transport properties enhanced by ionic liquids for CO_2 separation, RSC Adv., 7 (2017) 6422-6431.
[21] J.Y. Lim, J.K. Kim, C.S. Lee, J.M. Lee, J.H. Kim, Hybrid membranes of nanostructrual copolymer and ionic liquid for carbon dioxide capture, Chem. Eng. J., 322 (2017) 254-262.
[22] E. Hayashi, M.L. Thomas, K. Hashimoto, S. Tsuzuki, A. Ito, M. Watanabe, Application of Protic Ionic Liquids to CO_2 Separation in a Sulfonated Polyimide-Derived Ion Gel Membrane, ACS Appl. Polym. Mater., 1 (2019) 1579-1589.
[23] J. Han, L. Bai, S. Luo, B. Yang, Y. Bai, S. Zeng, X. Zhang, Ionic liquid cobalt complex as O_2 carrier in the PIM-1 membrane for O_2/N_2 separation, Sep. Purif. Technol.,

248 (2020) 117041.
[24] X. Yan, S. Anguille, M. Bendahan, P. Moulin, Ionic liquids combined with membrane separation processes: A review, Sep. Purif. Technol., 222 (2019) 230-253.
[25] W.A. Phillip, E. Martono, L. Chen, M.A. Hillmyer, E.L. Cussler, Seeking an ammonia selective membrane based on nanostructured sulfonated block copolymers, J. Membr. Sci., 337 (2009) 39-46.
[26] L. Ansaloni, Z. Dai, J.J. Ryan, K.P. Mineart, Q. Yu, K.T. Saud, M.-B. Hägg, R.J. Spontak, L. Deng, Solvent-Templated Block Ionomers for Base- and Acid-Gas Separations: Effect of Humidity on Ammonia and Carbon Dioxide Permeation, Adv. Mater. Interfaces, 4 (2017) 1700854.
[27] Zaripov, II, I.M. Davletbaeva, Z.Z. Faizulina, R.S. Davletbaev, A.T. Gubaidullin, A.A. Atlaskin, I.V. Vorotyntsev, Synthesis and Characterization of Novel Nanoporous Gl-POSS-Branched Polymeric Gas Separation Membranes, Membranes, 10 (2020) 25.
[28] L. Upadhyaya, A.Y. Gebreyohannes, F.H. Akhtar, G. Falca, V. Musteata, D.K. Mahalingam, R. Almansoury, K.C. Ng, S.P. Nunes, NEXARTM-coated hollow fibers for air dehumidification, J. Membr. Sci., 614 (2020) 118450.
[29] G.M. Shi, J. Zuo, S.H. Tang, S. Wei, T.S. Chung, Layer-by-layer (LbL) polyelectrolyte membrane with Nexar™ polymer as a polyanion for pervaporation dehydration of ethanol, Sep. Purif. Technol., 140 (2015) 13-22.
[30] Z. Dai, J. Deng, H. Aboukeila, J. Yan, L. Ansaloni, K.P. Mineart, M. Giacinti Baschetti, R.J. Spontak, L. Deng, Highly CO_2-permeable membranes derived from a midblock-sulfonated multiblock polymer after submersion in water, NPG Asia Materials, 11 (2019).
[31] F.H. Akhtar, H. Vovushua, L.F. Villalobos, R. Shevate, M. Kumar, S.P. Nunes, U. Schwingenschlögl, K.-V. Peinemann, Highways for water molecules: Interplay between nanostructure and water vapor transport in block copolymer membranes, J. Membr. Sci., 572 (2019) 641-649.
[32] F. Huang, T.D. Largier, W. Zheng, C.J. Cornelius, Pentablock copolymer morphology dependent transport and its impact upon film swelling, proton conductivity, hydrogen fuel cell operation, vanadium flow battery function, and electroactive actuator performance, J. Membr. Sci., 545 (2018) 1-10.
[33] Z. Dai, L. Ansaloni, J.J. Ryan, R.J. Spontak, L. Deng, Incorporation of an ionic liquid into a midblock-sulfonated multiblock polymer for CO_2 capture, J. Membr. Sci., 588 (2019) 117193.
[34] D. D'Angelo, S. Filice, A. Scarangella, D. Iannazzo, G. Compagnini, S. Scalese, Bi_2O_3/Nexar® polymer nanocomposite membranes for azo dyes removal by UV–vis or visible light irradiation, Catalysis Today, 321-322 (2019) 158-163.
[35] K.P. Mineart, B. Lee, R.J. Spontak, A Solvent-Vapor Approach toward the Control of Block Ionomer Morphologies, Macromolecules, 49 (2016) 3126-3137.
[36] K. Hashimoto, M. Hirasawa, H. Kokubo, R. Tamate, X. Li, M. Shibayama, M. Watanabe, Transport and Mechanical Properties of ABA-type Triblock Copolymer Ion Gels Correlated with Their Microstructures, Macromolecules, 52 (2019) 8430-8439.
[37] C. Makhloufi, D. Roizard, E. Favre, Reverse selective NH_3/CO_2 permeation in fluorinated polymers using membrane gas separation, J. Membr. Sci., 441 (2013) 63-

72.
[38] A. Raza, S. Farrukh, A. Hussain, Synthesis, Characterization and NH_3/N_2 Gas Permeation Study of Nanocomposite Membranes, J. Polym. Environ., 25 (2016) 46-55.